

Combination of Polygonatum and Scutellaria baicalensis triggers apoptosis through down-regulation of PON3-induced mitochondrial damage and endoplasmic reticulum stress in lung cancer cells

Haitao Liu

Shanghai Tenth People's Hospital

Liduo Yue

Shanghai Tenth People's Hospital

Yubin Li

Shanghai Tenth People's Hospital

Tiansheng Zheng

Tongji University School of Medicine

Wenjia Zhang

Shanghai Tenth People's Hospital

Chaoqun Li

Shanghai University of Sport

Wenbin Zhuang

Shanghai Tenth People's Hospital

Lihong Fan (≥ 1300008@Tongji.edu.cn)

Shanghai Tenth People's Hospital

Research Article

Keywords: Lung cancer, Polygonatum, Scutellaria baicalensis, Endoplasmic reticulum stress, Mitochondria, PON3, Reactive oxygen species

Posted Date: September 11th, 2023

DOI: https://doi.org/10.21203/rs.3.rs-3045676/v1

License: © ① This work is licensed under a Creative Commons Attribution 4.0 International License. Read Full License

Additional Declarations: No competing interests reported.

Page 2	2/33
--------	------

Abstract

Objective: Scutellaria baicalensis (SB) and polygonatum, two traditional Chinese medinces, are both known to suppress cancer. However, the mechanism and effect of combined treatment of them for lung cancer are rarely known. Investigating the combined effect of SB and polygonatum (hereafter referred to as HH) in potential mechanism of lung cancer is required.

Methods: Based on the theory of Chinese medicine and network pharmacology, In the in vivo experiment, a mouse model of carcinoma in situ was constructed and lung carcinoma in situ tissues were collected for proteomics analysis, ematoxylin-eosin staining and CK19 immunohistochemistry. In the in vitro experiment lung cancer A549 cells at logarithmic growth stage were taken and the inhibitory effect of HH on the proliferation of A549 cells was detected by CCK8 method. The expression of PON₃ was detected by quantitative polymerase chain reaction and Western Blot. In addition, the effect of HH on the induction of apoptosis in A549 cells and the changes of membrane potential and ROS content were detected by flow cytometry. The changes of PON₃ content in ER is observed by laser confocal microscopy, while the effects of HH on the expression of apoptosis-related proteins and ER stress-related proteins in A549 cells were examined by Western blot.

Result: By searching the TCMSP database and symmap database, the respective target genes of the double yellow were mapped into protein network interactions (PPI), and using Venn diagrams to show 38 genes in common between the double yellow and lung cancer, thus HH was found to play a role in the treatment of lung cancer. In vivo experiments showed that in a lung carcinoma in situ model, lung tumor tissue was significantly lower in the HH group compared to the control group, and PON_3 was shown to be downregulated by lung tissue proteomics analysis. The combination of HH was able to inhibit the proliferation of A549 cells in a concentration-dependent manner (P < 0.0001). The expression levels of apoptosis-related proteins and ER stress proteins were significantly increased and the expression levels of PON_3 could inhibit tumor cell proliferation (P < 0.0001). The combination of different concentrations of HH significantly induced apoptosis in A549 cells (P 0.05; P 0.0001), increased ROS content (P 0.01), and damaged mitochondrial membrane potential of A549 cells (P 0.05; P 0.0001), and significantly increased the expression levels of apoptosis-related proteins and ER stress proteins in lung cancer A549 cells.

Conclusion HH inhibits proliferation of lung cancer A549 cells by down-regulating PON3-induced apoptosis in the mitochondrial and ER pathways

Introduction

According to statistics, lung cancer continues to have the highest mortality rate of all cancers ^[1]. However, non-small cell lung cancer (NSCLC) is often chemoresistant and there is no reliable curative treatment. Further research is therefore needed to identify effective methods of treating NSCLC. Many herbs are closely related to lung cancer and show unique advantages in its treatment. Polygonatum is a perennial

herb of the genus, firstly published in the ancient Chinese book "The Book of Famous Doctors" [2]. It can strengthen middle-Jiao and Qi, tonify kidney and replenishing essence, nourish yin and moisturizing the lung, mainly for lung-dryness with nonproductive cough, body deficiency and hypodynamia, a chronic disease with dry teeth and body fluid deficiency. At the same time, it treats osteoporosis, diabetes and lung disease [3–5]. Scutellaria baicalensis is a traditional Chinese medicine (TCM) widely used in clinical practice. According to "Shennong's Classic of Materia Medica", it is a herb of the genus Scutellaria and is used as a medicine by its roots [6]. Modern pharmacology has proven that Scutellaria baicalensis has anti-inflammatory and anti-viral, anti-tumor, anti-cardiovascular and respiratory system diseases, etc. As natural products, two herbs have the effect of tonifying the lung and benefiting the qi, and both play an important role in the fight against tumors [7–8]. Traditional Chinese medicine (TCM), as a complementary and alternative medicine to western countries, is attracting global attention in the field of life sciences, and studies on the biomolecular mechanisms of TCM have been increasing in recent years. However, there are no studies on the effects of combining Polygonatum and Scutellaria baicalensis against lung cancer and their mechanisms at home and abroad.

Based on the "holistic view" of Chinese medicine and using the language of systems biology, network pharmacology explains the relationship between drugs and diseases from a multi-component and multi-directional perspective, which can visually represent the therapeutic characteristics of the components and improve the scientificity of the clinical use of traditional Chinese medicine^[9]. Therefore, we obtained the chemical composition of Polygonatum and Scutellaria baicalensis from the chemical composition database of traditional Chinese medicine, combined with the disease database to obtain the differentially expressed genes in lung cancer, to obtain the potential target of action of the combination of the two drugs in the treatment of lung cancer, and then used the bioinformatics software to enrich and analyse the potential target of action, to reveal the mechanism of HH.

PON, a protein of the oxyphosphatase family, is mainly found in the mitochondria and ER and has antioxidant and anti-inflammatory properties, regulating mitochondrial oxygen radicals $^{[10]}$, and recent studies have shown that PON₃ is highly expressed in tumors of the pancreas, bladder, thyroid, prostate, oral cavity, liver and testis and is localized in the mitochondria and ER, as well as in lung cancer $^{[11-12]}$. However, no specific mechanism of action and molecular biology related studies are available. Therefore, PON₃ can be used as a potential research target.

In this study, based on the theory of network pharmacology of traditional Chinese medicine, we combined Polygonatum as the main drug and Scutellaria baicalensis as an auxiliary drug in the ratio of $10:1^{[13]}$, constructed an animal model of lung carcinoma in situ, carried out proteomic analysis of lung tissues of mice treated with HH, and elucidated the effects of HH on inhibiting tumour development through PON_3 -mediated apoptosis through related experiments, as well as its molecular mechanism.

Results

1. Pharmacological Analysis Network of HH and HH inhibits lung cancer cell proliferation

Using the symmap database, we found that Polygonatum and SB (Fig. 1A) were closely related to lung cancer, non-small cell lung cancer (NSCLC) and lung adenocarcinoma (LA) (Fig. 1B), so we used the TCMSP database to search the active ingredients (Table 1) and the proteins contained in the two herbs, and combined with the lung cancer database to create a Venn diagram to find that there were 38 genes that intersected the three (Fig. 1C). The 244 potential targets were put into the STRING database, and we obtained the PPI network. We then put the network into Cytoscape software and analysed the Caspase family, HSP family, Bcl₂ family, AGC family, CDK family and PON family, which suggests that the mechanism of action of HH in treating NSCLC may be related to the regulation of these genes (Fig. 1D). In conclusion, these results suggest that HH has potential therapeutic effects on lung cancer.

Table 1 Main components of HH

Q	Scutellaria baicalensis	J	Polygonatum
Q1	acacetin	J1	(+)-syringaresinol
Q2	wogonin	J2	(+)-syringaresinol-o-beta-d-glucoside
Q3	(2r)-7-hydroxy-5-methoxy-2- phenylchroman-4-one	J3	(2r)-7-hydroxy-2-(4-hydroxyphenyl)chroman-4- one
Q4	5,7,2,5-tetrahydroxy-8,6- dimethoxyflavone	J4	(z)-1-(2,4-dihydroxyphenyl)-3-(4-hydroxyphenyl)prop-2-en-1-one
Q5	carthamidin	J5	(z)-nonadec-6-enoic acid
Q6	dihydrobaicalin_qt	J6	2-acridinecarboxylic acid
Q7	eriodyctiol	J7	Isoliquiritoside
Q8	salvigenin	J8	3'-methoxydaidzein
Q9	5,2',6'-trihydroxy-7,8- dimethoxyflavone	J9	4',5-dihydroxyflavone
Q10	5,7,2',6'-tetrahydroxyflavone	J10	1→2-β-D-glucopyranosidey
Q11	skullcapflavone ii	J11	4-methylolfurfural
Q12	oroxylin a	J12	apigenin
Q13	panicolin	J13	bgc
Q14	5,7,4'-trihydroxy-8-methoxyflavone	J14	dfv
Q15	neobaicalein	J15	diosgenin
Q16	dihydrooroxylin	J16	glucuronic acid
Q17	norwogonin	J17	gup
Q18	5,2'-dihydroxy-6,7,8- trimethoxyflavone	J18	hmf
Q19	ent-epicatechin	J19	isoliquiritigenin
Q20	stigmasterol	J20	neoliquiritin
Q21	coptisine	J21	oroxin a
Q22	bis[(2s)-2-ethylhexyl] benzene-1,2- dicarboxylate	J22	salicylic acid
Q23	diop	J23	sibiricoside
Q24	epiberberine	J24	sitogluside

Q	Scutellaria baicalensis	J	Polygonatum
Q1	acacetin	J1	(+)-syringaresinol
Q2	wogonin	J2	(+)-syringaresinol-o-beta-d-glucoside
Q25	moslosooflavone	J25	succinic acid
Q26	11,13-eicosadienoic acid, methyl ester	HH1	baicalein
Q27	5,7,4'-trihydroxy-6-methoxyflavanone	HH2	beta-sitosterol
Q28	5,7,4'-trihydroxy-8-methoxyflavanone	НН3	sitosterol
Q29	rivularin		

To initially investigate the proliferative effects of HH in A549 cells, A549 cells were exposed to different concentrations of HH for 24h and morphological and size changes were observed and cell viability was determined using the CCK8 colorimetric assay. The results found HH inhibited the proliferation of A549 cells in a dose-dependent manner with an IC_{50} value of approximately 4.25 mg/mL (Fig. 1E). Apprently, we tested the IC_{50} of the two single drugs separately and found that HH required fewer concentrations of both drugs to kill the same number of A549 cells(Fig. 1F). HH observed severe morphological changes in the cells under phase contrast microscopy, including rounding and atrophy, accompanied by a decrease in the number of cells (Fig. 1G). Thus, these data suggest that HH inhibited the proliferation of A549 cells and that a lower concentration of drug was required to inhibit the proliferation of the same number of A549 cells with HH compared to the two single agents.

2. HH suppresses tumor growth in vivo

To test the inhibition of HH in vivo, mice were constructed with Kras^{LSL-G12D}/p53^{flox/flox} as a lung carcinoma in situ model, and the groups were divided into blank group, cre group and HH group. As shown in the figure (Fig. 2A), Kras^{LSL-G12D}/p53^{flox/flox} mice formed carcinoma in situ in the lung after 4 weeks of intranasal drops of cre virus and were treated with HH. Mice were then executed after 4 weeks and lung tissue was collected. The volume of lung carcinoma in situ tissue in the HH-treated group was significantly smaller than that in the control group (Fig. 2B). The lung tissues were sectioned and subjected to HE staining and CK19 IHC analysis, and tumour growth was significantly inhibited after HH treatment compared to the control group (Fig. 2C-D). Notably, there was no significant change in the body weight of the animals in both groups (**Figure S1**). The above data suggest that HH can inhibit the growth of tumour tissue in the Kras^{LSL-G12D}/p53^{flox/flox} construct lung carcinoma in situ model.

To further explore the mechanism of the inhibitory effect of HH on murine lung carcinoma in situ, the remaining lung tissues were subjected to proteomic analysis. A series of proteins with differential expression levels were screened by corrected FDR values < 0.05 and log2FC > 1 from 2133 proteins plotted as volcanoes, of which 235 were upregulated and 341 downregulated in the HH group (**Figure S2**). The 23 proteins (Table 2) with higher differential values were then filtered into heat map analysis and found that

Sptbn1, Serpinb9, Armcx3, Csgalnact2, Tgm1, Klf15, Tbkbp1, Cast were the up-regulated proteins, and Tle2, Fasn, Paqr8, Smim24, Lsp1, Dpp9, Tle6, Fmo2, Lmo7, Cfap52, Gnb2, Arhgef16, Paf1, Gpank1 were the down-regulated proteins (Fig. 2E). Notably, among the down-regulated proteins, PON_3 had the largest difference value compared to controls. In the TCGA database, it was found that the expression level of PON_3 was significantly higher in lung adenocarcinoma patients compared to normal subjects (Fig. 2F), and a pan-cancer analysis of PON_3 using the GEPIA2 database revealed that it was expressed at high levels in most tumours (**Figure S3**). These results indicate that the expression level of PON_3 in the HH-treated group was significantly lower than that in the control group in lung cancer.

Table 2
Differentially expressed proteins between HH and Control groups

ID	gene	padj	log2FC(HJ+HQ/con)
Q5D002	Sptbn1	<0.0001	9.699771
P5045 ₃	Serpinb9	<0.0001	8.410736
Q9UH62	Armcx3	<0.0001	7.358286
Q8N6G5	Csgalnact2	<0.0001	7.196194
Q9JLF6	Tgm1	<0.0001	7.057266
Q9UIH9	Klf15	<0.0001	6.884321
A7MCY6	Tbkbp1	<0.01	6.381669
Q8WTX7	Cast	<0.0001	6.321527
Q04725	Tle2	<0.05	-1.76326
P49327	Fasn	<0.05	-1.95848
Q8TEZ7	Paqr8	<0.0001	-2.29414
075264	Smim24	<0.05	-2.3136
P33241	Lsp1	<0.05	-2.33041
Q86TI2	Dpp9	<0.01	-2.33495
Q9H808	Tle6	<0.01	-2.40362
Q99518	Fmo2	<0.05	-3.29606
Q8WWI1	Lmo7	<0.05	-3.38343
Q8N1V2	Cfap52	<0.05	-3.50771
P62879	Gnb2	<0.0001	-3.68185
Q5VV41	Arhgef16	<0.0001	-3.73151
Q8N7H5	Paf1	<0.01	-3.84144
095872	Gpank1	<0.0001	-4.80342
Q15166	Pon3	<0.01	-5.87236
	·	·	

3. HH inhibits the expression of PON and induces apoptosis

In vitro experiments revealed a concentration-dependent decrease in the expression of PON₃, both at the transcriptional and protein levels, after HH intervention compared to the control group (Fig. 3A-B). A549 cells were also subjected to a similar concentration-dependent decrease in PON₃ transcript levels after different periods of HH intervention (Fig. 3A). Apoptosis is thought to be one of the main causes of cell growth inhibition. Phosphatidylserine ectopia and loss of cell membrane integrity are the main features of apoptosis. First, we investigated the effect of HH on apoptosis in A549 cells using a membrane linked protein FITC/PI double staining kit and flow cytometry. The data showed that HH induced apoptosis in a dose and time-dependent manner in A549 cells (Fig. 3E). To investigate whether PON₃ is involved in the inhibitory effect of HH on lung cancer cells, we knocked down PON3 by siRNA (Fig. 3C-D), and then compared with siRNA-control, we found that the proliferation of A549 cells was greatly reduced and it can increase apoptosis after flow cytometry and CCK8 experiments (Fig. 3F, 4D), indicating that knockdown of PON₃ has an inhibitory effect on the proliferation of lung cancer cells. In conclusion, HH can induce apoptosis in A549 cells by down-regulating PON₃.

4. HH induces apoptosis via ROS in A549 cells

Reactive oxygen species (ROS), produced by eukaryotic cells through aerobic metabolism, are byproducts of cellular respiration, are highly reactive and have a crucial role in human physiological and pathological processes. Adequate amounts of ROS can maintain the physiological requirements of human cells and tissues, participate in cellular metabolic regulation and stress responses, control normal cell proliferation and differentiation, and support cellular adaptation to changing environments and stresses [14]. However, the accumulation of abnormal ROS can lead to a loss of control of the cellular antioxidant defense system, and toxic levels of ROS in tumor cells have been shown to exert anti-tumor effects by increasing oxidative stress and inducing tumor cell death [15]. Therefore, we used the ROSsensitive fluorescent DCFH-DA to analyse intracellular ROS production. Analysis by flow cytometry showed that after incubation of A549 cells with HH for 24h, the FITC fluorescence intensity of the cells was significantly enhanced and showed time and concentration dependence (Fig. 4A-B). To determine whether ROS contributed to HH-induced cell death, we treated cells with the ROS scavenger Nacetylcysteine (NAC). CCK8 analysis showed that NAC reduced HH-induced cell death (Fig. 4C), and Annexin V/PI staining analysis also confirmed that NAC attenuated HH-induced apoptosis. We also found that the apoptosis rate of A549 cells knocked down by PON₃ increased after the addition of NAC (Fig. 4D), while interestingly, transfection of plasmids overexpressing PON₃ into A549 cells with the intervention of HH reversed the level of ROS in line with the results after the addition of NAC(Figure 4E). The above results suggest that ROS plays an important role in the proliferation of A549 and is able to induce apoptosis in lung cancer cells, while being downstream of PON₃.

5. HH apoptosis by the mitochondrial pathway via PON₃

To further investigate whether HH induces apoptosis in A549 cells via the mitochondrial pathway, we analysed the effects of HH on mitochondrial membrane potential and Bcl family proteins. Mitochondrial

membrane potential is an important indicator of mitochondrial function, and a decrease in membrane potential can lead to mitochondrial apoptosis. Therefore, we measured mitochondrial membrane potential by flow cytometry and found that Hh-treated cells exhibited increased red fluorescence intensity and decreased green fluorescence intensity, whereas A549 cells exhibited a concentration-dependent decrease in mitochondrial membrane potential. (Fig. 5A). Western blot and qPCR also showed that the expression of cleaved caspase 3 and Bax/Bcl2 in A549 cells increased in a concentration-dependent manner after HH intervention (Fig. 5D). After knocking out PON₃, Bax mRNA expression was upregulated and Bcl2 mRNA expression was downregulated (Fig. 5B-C). A past study showed that showed that PON₃ was present in the mitochondria of A549 after purification of mitochondria by differential centrifugation using protein blotting^[11]. Therefore, we hypothesized that HH could cause the mitochondria to lose their antioxidant capacity by decreasing PON₃, leading to an increase in ROS, disrupting the mitochondrial membrane potential and inducing apoptosis in the mitochondrial pathway.

6. HH induces apoptosis by triggering endoplasmic reticulum stress via PON₃

Previous studies^[11] found that PON₃ was localized in mitochondria and ER in hepatocellular carcinoma cells HEK293 and localization in lung A549 has not been visualized. In this experiment, we intervened in A549 cells by HH group (4mg/mL) for 24h, loaded ER probe together with control group and incubated with primary antibody PON₃ and secondary antibody, and finally the anti-quenching agent containing DAPI sealed the slices after co PON₃ was found to be present in the ER under confocal microscopy, and the expression of PON₃ on the ER was significantly lower in the HH group than in the control group (Fig. 6A). The ER plays an important role in protein synthesis, modification, processing, and transport, as well as calcium homeostasis [16]. Various cellular stresses can lead to the accumulation of unfolded and misfolded proteins in the lumen of the ER, a condition known as endoplasmic reticulum stress (ERS) [17]. To prevent or respond to ER, cells have integrated signaling systems to restore homeostasis and normal ER function. The basic pathways that make up the components of this response include the unfolded protein response (UPR), ER-associated degradation (ERAD), autophagy, hypoxic signaling and mitochondrial biogenesis [18]. Among these is the UPR, a homeostatic signaling network that coordinates the restoration of ER function, and failure to adapt to external stimuli to initiate ER stress can lead to apoptosis. It has three important sensors: inositol-dependent kinase 1α (IRE1), protein kinase R-like endoplasmic reticulum kinase (PERK) and activating transcription factor 6 (ATF6), transmembrane proteins associated with the ER [19-20]. These proteins, in turn, are sensed by the ER's molecular chaperone glucose regulatory protein 78 (GRP78), which promotes protein folding and assembly, controls protein mass, and regulates ER stress signaling via Ca^{2+ [21]}. Upon release of GRP78, PERK acts similarly to IRE1, leading to dimerization and phosphorylation of the eukaryotic translation initiation factor 2α(eIF2α) promoter, thereby inhibiting overall protein synthesis [22]. Phosphorylation of eIF2a activates activating transcription factor 4 (ATF4), which controls the expression of apoptosis-associated ERSspecific transcription factors, namely growth arrest and DNA injury-inducible gene 153 (CHOP), to regulate the UPR $^{[23-26]}$, and CHOP can act as a characteristic protein of the ER, initiating a pro-apoptotic program to promote apoptosis $^{[27]}$. More importantly, ERS is closely related to the development of lung cancer. To further assess whether ER stress was involved in the mechanism of HH-induced apoptosis in human lung cancer A549 cells, we measured ER stress receptors and specific markers. The expression levels of ATF4 and CHOP were found to be higher than the control in the transcriptional level (Fig. 6B-C). Western blot analysis showed that GRP78, CHOP, p-perk, ATF4, p-elF2 α , and caspase 12 protein levels were elevated after HH treatment, while perk,-elF2 α protein levels were not significantly altered (Fig. 6D). Meanwhile, we observed the expression of related proteins at transcriptome level using A549 cells after knockdown of PON₃, and the results showed that the expression of ATF4 and CHOP was up-regulated and there were statistically significant differences (Fig. 6B-C). To verify whether HH induces ER stress via PON3, we subjected A549 cells after knockdown of PON3 to protein blotting analysis. The results revealed a trend consistent with the HH intervention compared to the control (Fig. 6E). Correspondingly, Cheng $^{[28]}$ et al. found that reactive oxygen species could mediate ER stress to induce apoptosis in NSCLC, and CHOP is a core protein of ER stress, so we hypothesized that HH could induce apoptosis by inhibiting PON₃ leading to elevated ROS and over-stimulation of ER to cause ER stress in A549 cells.

Disccusion

Apart from the standard treatment for lung cancer, Chinese traditional medicine is known for its multitarget and low side effects, and has a great advantage in improving the molecular biological behaviour of lung cancer cells ^[29]. According to TCM theory, when the body's immunity is too weak and the tumour's ability to grow is too strong, the imbalance is regulated by "strengthening the body" and "removing the evil", with "strengthening the body" referring to enhancing the body's anti-cancer The "strengthening of the body" refers to enhancing the body's immunity against cancer, while "removing evil" refers to inhibiting the growth, proliferation, invasion and migration of tumor cells ^[29]. Based on different Chinese medicine databases and network pharmacology, it was found that both Polygonatum and Scutellaria baicalensis have therapeutic effects on lung cancer. Therefore, in vivo and in vitro experiments were conducted to determine the effects of HH in combination with PON₃ on lung cancer and to explore their potential mechanisms of action.

In this paper, we firstly determined that HH could inhibit the proliferation of lung cancer A549 cells at certain concentrations in a dose-dependent manner by CCK8 assay and microscopic observation, and clarified the therapeutic effect of double Scutellaria in lung cancer, and also established a lung in situ cancer model using the conditional allele of Kras^{LSL-G12D}/p53f^{lox/flox} after subjecting lung tissues to HE staining and CK19 IHC analysis was performed to illustrate the anti-tumour effects of HH in in vivo studies. To further explore the mechanism of HH in treating lung cancer, proteomic analysis using the lung tissues showed reduced expression of PON₃ in the HH group. As the TCGA database search revealed significant differences in PON₃ expression levels between normal subjects and lung cancer patients, we next verified that PON₃ was highly expressed in lung cancer by quantitative polymerase chain reaction and protein immunoblotting, and that HH was able to down-regulate PON₃ expression in lung cancer after

flow cytometry and CCK8 experiments, which revealed that HH induced apoptosis in a concentration-dependent manner in contrast, the proliferation of A549 cells was greatly reduced by PON₃ knockdown, and apoptosis was also reduced. Therefore, we demonstrate that HH induces apoptosis in lung cancer cells by down-regulating the expression level of PON₃.

Previous studies $^{[12]}$ have shown that PON_3 is able to localize to the mitochondrial membrane and prevent the formation of ${\rm O_2}^-$ on both sides of the membrane, implying that ${\rm PON_3}$ acts on or regulates coenzyme Q10 (CoQ10) to prevent ${\rm O_2}^-$ formation. When mitochondria produce excess superoxide, it leads to peroxidation of the mitochondria-specific lipid cardiolipin. This disrupts the interaction of cardiolipin with cytochrome c, producing a soluble component of the latter. Together with the outer mitochondrial membrane permeability of Bax, this causes loss of membrane potential and release of cytochrome c, ultimately inducing apoptosis. We then performed JC-1 probe membrane potential and reactive oxygen species assays and found that after HH intervention, the membrane potential of lung cancer A549 cells decreased and reactive oxygen species content increased, both in a concentration-dependent manner, and our study revealed that CCK8 analysis and flow cytometry showed that NAC reverses HH-induced apoptosis. More interstingly, A549 cells with knockdown of PON₃ showed increased apoptosis after addition of NAC, suggesting that ROS is downstream of PON3, and protein blotting revealed elevated protein levels of Bax/Bcl₂ and cleaved-caspase 3. And PON₃ overexpression was able to reverse the increase in ROS levels after HH intervention Through the above data we concluded that HH can downregulate PON₃, inhibit the antioxidant effect of PON₃ and cause an increase in reactive oxygen species in mitochondria, thus destroying the mitochondrial membrane within mitochondria, leading to excessive accumulation of ROS, cellular dysfunction and ultimately apoptosis. It was also found that PON₃ was also distributed in the ER at the same time, which we verified by confocal laser microscopy localization observation and found that the expression of PON₃ decreased significantly after dosing treatment. To investigate whether apoptosis after HH treatment was related to ER stress, we measured ER stress receptors and specific markers. Protein blot analysis showed that GRP78, CHOP, p-perk, ATF4, p-eIF2a, and caspase12 protein levels were elevated after HH intervention, and the same result was obtained after knocking down PON₃. The results of quantitative polymerase chain reaction also showed that the expression levels of CHOP, ATF4, Bax and Bcl2 after treatment with knockdown PON3 followed the same trend as those after HH treatment.

In summary, our results suggest that HH can inhibit the antioxidant effect of lung cancer A549 cells by downregulating PON3 in mitochondria, causing excessive accumulation of ROS in mitochondria, disrupting the mitochondrial membrane potential, releasing ROS into the cytoplasm to the endoplasmic reticulum of the cytoplasm, and excessive ROS stimulates the endoplasmic reticulum triggering endoplasmic reticulum stress, as well as apoptosis in the endoplasmic reticulum and mitochondrial pathways (Fig. 7). This finding will provide evidence of the therapeutic potential of HH for NSCLC patients and new therapeutic strategies for the clinical management of lung cancer patients.

HH downregulates PON₃ expression, then the inhibition of ROS by PON₃ is lifted, resulting in excessive accumulation of ROS in the mitochondria and decreasing MMP. At the next stage, excess ROS is released to stimulate the ER to trigger ER stress. Finally, apoptosis of lung cancer cells was induced by two pathways: ER stress and mitochondrial apoptosis.

Materials and Method Animal study

We established a lung adenocarcinoma model in 12 mice (Shanghai Slack Experimental Animal Center Laboratory Animal Co.,Ltd, Shanghai, China) using the conditional allele Kras^{LSL-G12D}/p53^{flox/flox}. All experiments were performed in accordance with the Animal Care Guidelines of Tongji University Animal Care and Use Committee. Adenovirus of 1*10⁶ pfu was added to the buffer drop into the nasal cavity of each Kras^{LSL-G12D}/p53 flox/flox mouse and used to construct a lung carcinoma in situ model, while administered in chow and monitored for status on alternate days. At the same time, 12 mice were randomly divided into HH group, control group and dummy group. After the three groups of mice were isolated, they were further placed under SPF conditions, and the mental and tumor status were observed every day. Approximately one week after titration of the adenovirus, the diet of animals in the HH group was changed to a specific diet when lung carcinoma in situ formed. The special feed is produced by Wuxi Fanbo Biotechnology Co., Ltd (Wuxi, China) and is supplemented with 12.13g of Polygonatum and 1.213g of Scutellaria baicalensis per kg of common feed. All mice were executed after 6 weeks of treatment and lung tissue was collected for transcriptional and proteomic analysis and fixed in 4% paraformaldehyde for immunohistochemical (IHC) analysis.

Cell culture and reagents

The A549 cells line was provided by the Cell Bank of Shanghai Institute of Cell Biology. RPMI 1640 medium containing 10% neonatal calf serum and 100 U/ml penicillin-streptomycin diabody (Gibco, NY, USA) was used as a complete medium. A549 cells were grown in complete medium and constant temperature incubator at 37°C and 5% CO₂, respectively. Cells were subcultured at 2–3 day intervals.

Network pharmacological analysis of HH/ HH active ingredient and lung cancer target collection

Link between lung cancer and Polygonatum and Scutellaria baicalensis identified through symmap database (http://www.symmap.org/). The TCMSP (https://tcmspw.com/)was searched and the active ingredients and corresponding targets were obtained based on pharmacokinetic parameters with oral bioavailability (OB) \geq 30% and drug similarity (DL) \geq 0.18. NSCLC targets were collected by searching drugbank, OMIM and GeenCards databases, combined with uniprot's human-derived gene database to build a database for non-small cell lung cancer, and using Venn diagrams https://www.vandepeerlab.org/to map HH and NSCLC interacting genes. Drug composition and target analysis mapping of HH using Cytoscape.3.9.

HH treatment

According to the clinical indications, the daily dose of Polygonatum drinking tablets was 30 g and the daily dose of SB drinking tablets was 6 g. In this experiment, concentrated granules of Polygonatum and SB(Jiangyin Tianjiang Pharmaceutical, Jiangyin, China) were used, in which 4 g of Polygonatum concentrated granules were equivalent to 10 g of Polygonatum drinking tablets and 2 g of concentrated Sb granules were equivalent to 10 g of Sb drinking tablets in the ratio of 10:1 in agreement with the decoction of Polygonatum and Sb in the ratio of 5:1. HH The concentrations of the granules were 4m g/m L and 8mg/m L. In animal experiments, the dose of HH to mice (g) was: mouse daily dose = 9.1 x human daily dose/60 kg. Therefore, HH feed was produced by Wuxi Fanbo Biotechnology Company with 1 kg normal feed supplemented with 12.13g polygonatum and 1.213g SB.

Histological assessments

Lung tumor tissues were fixed in situ in 10% formaldehyde and embedded in paraffin. Sections were sectioned at 4 μ m, baked at 70°C for 4 hours, dehydrated using a graded ethanol series, and stained with hematoxylin and eosin (HE). For immunohistochemical staining, tissue was overlaid with 3% H_2O_2 for 15 minutes at room temperature, followed by heating in citrate buffer for 15 minutes for antigen retrieval. Sections were then blocked with 5% bovine serum albumin in Tris-buffered saline for 30 minutes and incubated with CK19 antibody overnight at 4°C. Sections were stained with diluted Streptavidin Peroxidase-Horseradish (HRP) Stain Kit and mixed with diluted Streptavidin Peroxidase-HRP at room temperature. Sections were counterstained with HE for 3 min and analyzed under a phase-contrast microscope.

Cell proliferation assay

A549 cells at logarithmic growth stage were digested with trypsin and prepared into cell

suspensions at a density of 1×10^4 /mL, inoculated into 96-well cell culture plates at 100 µL per well and incubated in an incubator for 24 h. HH groups were treated with final concentrations of 2, 4, 6, 8 and 16 mg/mL, while control groups were given equal volumes of culture medium. incubation. After 24h of drug treatment, 10μ L of LCCK-8 working solution and 90μ L of serum-free RPMI-1640 medium were added to each well, and incubated in the incubator for 30min. Then use an automatic microplate reader to record the optical density (OD) of each well at 450nm, and calculate the cell viability. Cell survival rate=(OD treatment group-OD blank group)/(OD control group-OD blank group)×100%.

Analysis of gene expression by quantitative RT-PCR (qRT-PCR)

Total RNA was extracted using the FastPure Cell Total RNA Isolation Kit (Vazyme, RC101-01, China), and 2 µg of total RNA was prepared using the cDNA Synthesis System Kit (Vazyme, R211-01, China). RT−QPCR was performed on a CFX384™ Real-Time System (Biorad Laboratories, California, USA) using 2×SYBRGreenqPCR MasterMix (ROX2p) (Vazyme, Q421-02, China). The unit is programmed according to

the following protocol: cDNA amplification: 94°C for 20 s. Denature at 60 – 58°C for 30 s. Anneal at 72°C for 30 seconds, 40 cycles. Melting curve analysis: 95°C for 15 seconds. Incubate at 60°C for 1 min. Store at 95°C for 30 seconds Primer sequences are: PON₃ (forward, 5'- GGATCACAGTCTCAGCAGACCA-3', reverse, 5'- GTCAGGTTATCCACTAAGGTGCC-3'), ATF4 (forward, 5'- TTCTCCAGCGACAAGGCTAAGG-3', reverse, 5'- CTCCAACATCCAATCTGTCCCG-3'), CHOP (forward, 5'- GGTATGAGGACCTGCAAGAGGT-3', reverse, 5'- CTTGTGACCTCTGCTGGTTCTG-3'), Bcl-2 (forward, 5'- ATCGCCCTGTGGATGACTGAGT-3', reverse, 5'- GCCAGGAGAAATCAAACAGAGGC-3'), Bax (forward, 5'- TCAGGATGCGTCCACCAAGAG-3, reverse, 5'- TGTGTCCACGGCGCAATCATC-3'), GAPDH(forward, 5'-GATTCCACCCATGGCAAATTC-3', reverse, 5'-GTCATGAGTCCTTCCACGATAC-3').

Western blotting (WB)

A549 cells at logarithmic growth stage were inoculated into 6-well plates at a density of 5×10^5 /mL for 24 h. Cells were treated with different concentrations of HH for 24 h. After removal of medium, cells were washed 3 times with cold PBS (pH 7.4) and lysed in RIPA buffer supplemented with phenylmethylsulfonyl fluoride (PMSF) and phosphatase inhibitors. The lysates were incubated on ice for 30 min, centrifuged at 12,000 rpm for 10 min at 4°C, and the protein concentration in whole cell lysates was quantified using a BCA kit (20201ES76, YEASEN, China). Proteins were separated by sodium dodecyl sulfate-polyacrylamide gel electrophoresis (SDS-PAGE) and transferred to nitrocellulose (NC) membranes. Nonspecific binding was blocked with 5% bovine serum albumin (BSA) for 1 hour at room temperature. Then incubate the membrane with the primary antibody overnight at 4°C (anti-PON₃, anti-CHOP, anti-elF2 α , anti-p-elF2 α , PERK, anti-p-PERK, anti-GRP78, anti-ATF4, anti-Bax, anti-caspase 12, anti-cleaved-caspase 3, anti-Bcl₂) and antibody to β -actin. It was then incubated with secondary antibody dilutions for 1 hour at room temperature. Finally, the protein expression level was measured using ECL kit (SQ101L, Epizyme Biomedical Technology Company, China). All antibodies were purchased from Cell Signaling Technologies and diluted 1:1000.

Mitochondrial membrane potential assay

Mitochondrial membrane potential (MMP) was detected using JC-1 detection kit (40706ES60, YEASEN, China). Cells were washed once with PBS solution. Add 1 mL of cell culture medium and 1 mL of JC-1 staining solution to each well, and mix well. Place the cells in a cell incubator and incubate at 37°C for 20 minutes, the supernatant was then aspirated. The supernatant was then aspirated and washed twice with JC-1 staining buffer. Choose an appropriate amount of JC-1 Staining Buffer (1X) to resuspend the cells. Mitochondrial membrane potential was recorded by flow cytometry at an excitation wavelength of 490 nm and an emission wavelength of 530 nm.

ROS measurement

Cells were inoculated in 6-well culture plates to ensure 50-70% cell confluence at the time of assay. After 24 h of drug treatment, the cell culture medium was aspirated and the appropriate volume of diluted DCFH-DA working solution was added to 1 mL. The cells were incubated for 30 min at $_37\%$ in a cell culture incubator protected from light. The cells were washed once or twice with serum-free RPMI-1640

culture medium to remove the DCFH-DA that had not entered the cells, and finally 500 mL PBS buffer was added. After resuspension, the ROS level was detected by flow cytometry at 488 nm excitation wavelength and 525 nm emission wavelength.

Apoptosis detection

A549 cells were seeded into 6-well culture plates. After the cell fusion rate reached 70%, the wells of each drug group were treated with different concentrations of HH (4 and 8 mg/ml) for 24 hours, resuspended at 105° C, and centrifuged at 1000g for 5 minutes. discard the supernatant, add 195μ Lannexin V-FITC conjugate to suspend the cells. Add 5 μ L Annexin V-FITC and mix gently. Add 10μ l of propidium iodide staining solution. Incubate at room temperature for 15μ c minutes in the dark. Cells were resuspended twice during incubation, placed in an ice bath and covered with aluminum foil.

ER fluorescent probe loading

Cell culture medium was removed and cells grown on coverslips were washed with PBS. Remove wash solution, add ER-Tracker Red, warm to 37°C, and incubate with cells at 37°C for 30 minutes. Remove the red ER-Tracker dye and wash the cells twice with cell culture medium. Fix for 2 minutes at 37°C using 4% formaldehyde. After fixation, wash 3 times with appropriate washing solution for 5 minutes each.

Immunocytochemistry

Control cells and A549 cells treated with Shuanghuang for 24 hours were fixed with 4% paraformaldehyde at room temperature, permeabilized with permeabilization solution, and blocked with 3% BSA for 18 minutes at room temperature. After blocking, PON₃-GFP was added and incubated for 1 hour at 37°C in a cell culture incubator.

Cell transfection

The siRNA oligonucleotides were synthesised by Hanheng Biologicals (Shanghai, China). Cells were transfected with small interfering RNAs targeting PON₃ or control group siRNAs using Lipofectamine™ RNAiMAX (Hanheng Bio, Shanghai, China) according to the manufacturer's instructions. Briefly, the cells were placed in 6-well plates at a density of of 5×10⁴ for 24 hours, and then transfected with 100 nM PON₃ or control siRNA. after 6 hours the medium was replaced with fresh medium and the cells were incubated for a further 42 hours. In subsequent experiments, cells were treated with 4 mg/ml HH for 24 hours. PON3 overexpression plasmid (OE-PON₃) and its negative control (OE-NC) were purchased from Genechem (Shanghai, China).

Statistical analysis

All data are presented as mean ± standard deviation (SD). Analysis was performed using GraphPad Prism 8.2 software. Significant differences were determined by one-way analysis of variance. Differences between groups were determined by Tukey's multiple comparison post hoc test. A p-value < 0.05 was considered statistically significant.

Abbreviations

SB Scutellaria baicalensis ER endoplasmic reticulum НН Scutellaria baicalensis and polygonatum protein network interactions **ERS** endoplasmic reticulum stress **UPR** unfolded protein response **ERAD** endoplasmic reticulum-associated degradation IRE1 inositol-dependent kinase 1a **PERK** protein kinase R-like endoplasmic reticulum kinase ATF6 activating transcription factor 6 GRP78 glucose regulatory protein 78 elF2α eukaryotic translation initiation factor 2a ATF4 activating transcription factor 4 CHOP growth arrest and DNA injury-inducible gene 153 ROS reactive oxygen species IHC immunohistochemical OB oral bioavailability DL drug similarity HRP

horseradish peroxidase

HE

hematoxylin-eosin staining

OD

optical density

SDS-PAGE

sodium dodecyl sulfate-polyacrylamide gel electrophoresis

BSA

bovine serum albumin

PMSF

Phenylmethanesulfonyl fluoride

MMP

Mitochondrial membrane potential

NSCLC

non-small cell lung cancer

LA

lung adenocarcinoma

NAC

N-acetylcysteine

CoQ10

coenzyme Q10

Declarations

Author Contributions

L. H. F. and H. T. L. designed the experiments; H. T. L., C. Q. L. and W. B. Z. performed experiments; Y. B. L. and H. T. L. analyzed experiments; L. D. Y. and L. H. F. supervised the

study; H. T. L. and L. D. Y.wrote the manuscript with input from T. S. Z., H. T. L., W. J. Zand

L. H. F. All authors have read and approved the article.

Funding

This research project was supported by the International Cooperation Project of the

Belt and Road (No. 20400750600)

Data availability

The data analyzed during the current study are available from the corresponding author upon reasonable request.

Ethics approval

All animal experiments were approved by the Animal Ethics Committees of Shanghai Tenth People's Hospital.

Consent for publication

Not applicable.

Conflict of Interest

The authors declared that they have no conflicts of interest to this work.

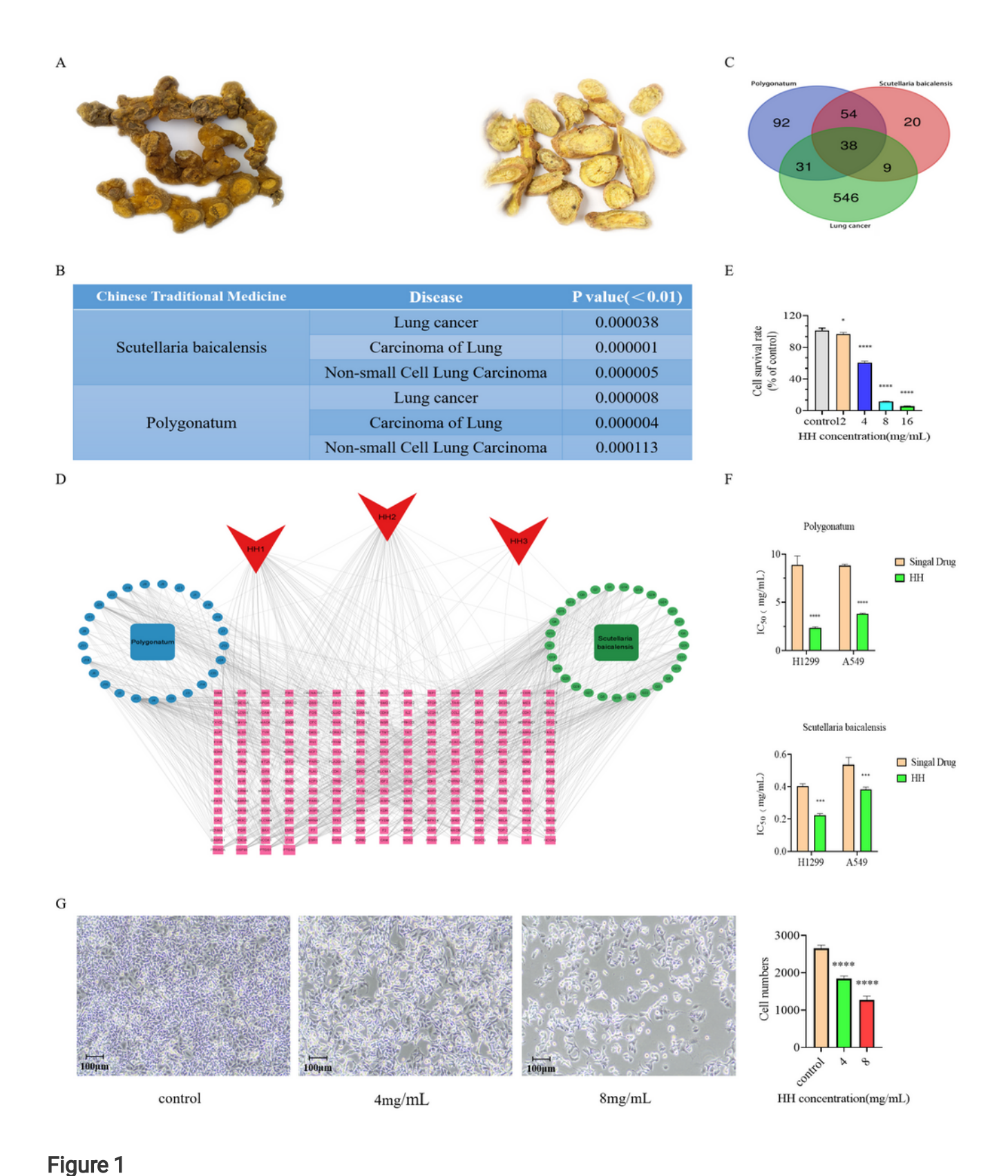
References

- 1. Siegel RL, Miller KD, Wagle NS, Jemal A. Cancer statistics, 2023. CA Cancer J Clin. 2023;73(1):17-48.
- 2. Zhao L, Xu C, Zhou W et al. Polygonati Rhizoma with the homology of medicine and food: A review of ethnopharmacology, botany, phytochemistry, pharmacology and applications. J Ethnopharmacol.
- 3. Zhao J, Lin F, Liang G, et al. Exploration of the Molecular Mechanism of Polygonati Rhizoma in the Treatment of Osteoporosis Based on Network Pharmacology and Molecular Docking. Front Endocrinol (Lausanne). 2022;12:815891. Published 2022 Jan 5.
- 4. Xie Y, Mu C, Kazybay B, et al. Network pharmacology and experimental investigation of Rhizoma polygonati extract targeted kinase with herbzyme activity for potent drug delivery. Drug Deliv. 2021;28(1):2187–97.
- 5. Gu X, Zhu LY, Xu ZY, Shen KP. Astragaloside IV and Saponins of Rhizoma Polygonati Cure Cyclophosphamide-Induced Myelosuppression in Lung Adenocarcinoma via Down-Regulating miR-142-3p. Front Oncol. 2021;11:630921.
- 6. Zhao T, Tang H, Xie L, et al. Scutellaria baicalensis Georgi. (Lamiaceae): a review of its traditional uses, botany, phytochemistry, pharmacology and toxicology. J Pharm Pharmacol. 2019;71(9):1353–69.
- 7. Yu P, Li J, Luo Y et al. Mechanistic Role of Scutellaria baicalensis Georgi in Breast Cancer Therapy [published online ahead of print, 2023 Jan 18]. Am J Chin Med. 2023;1–30.
- 8. Li L, Thakur K, Cao YY, Liao BY, Zhang JG, Wei ZJ. Anticancerous potential of polysaccharides sequentially extracted from Polygonatum cyrtonema Hua in Human cervical cancer Hela cells. Int J Biol Macromol. 2020;148:843–50.
- 9. Wu SS, Hao LJ, Shi YY, et al. Network Pharmacology-Based Analysis on the Effects and Mechanism of the Wang-Bi Capsule for Rheumatoid Arthritis and Osteoarthritis. ACS Omega. 2022;7(9):7825–36.
- 10. Bacchetti T, Ferretti G, Sahebkar A. The role of paraoxonase in cancer. Semin Cancer Biol. 2019;56:72–86.

- 11. Schweikert EM, Devarajan A, Witte I, et al. PON3 is upregulated in cancer tissues and protects against mitochondrial superoxide-mediated cell death. Cell Death Differ. 2012;19(9):1549-60.
- 12. Zhu L, Shen Y, Sun W. Paraoxonase 3 promotes cell proliferation and metastasis by PI3K/Akt in oral squamous cell carcinoma. Biomed Pharmacother. 2017;85:712–7.
- 13. Zhang J, Wang YZ, Yang WZ, Yang MQ, Zhang JY. Research progress in chemical constituents in plants of Polygonatum and their pharmacological effects. Zhongguo Zhong Yao Za Zhi. 2019;44(10):1989–2008. Chinese.
- 14. Zhou B, Zhang JY, Liu XS, et al. Tom20 senses iron-activated ROS signaling to promote melanoma cell pyroptosis. Cell Res. 2018;28(12):1171–85.
- 15. Harris IS, DeNicola GM. The Complex Interplay between Antioxidants and ROS in Cancer. Trends Cell Biol. 2020;30(6):440–51.
- 16. Parashar S, Ferro-Novick S. Architecture of the endoplasmic reticulum plays a role in proteostasis. Autophagy. 2022;18(4):937–8.
- 17. Chen X, Cubillos-Ruiz JR. Endoplasmic reticulum stress signals in the tumour and its microenvironment. Nat Rev Cancer. 2021;21(2):71–88.
- 18. Yang Z, Huo Y, Zhou S, et al. Cancer cell-intrinsic XBP1 drives immunosuppressive reprogramming of intratumoral myeloid cells by promoting cholesterol production. Cell Metab. 2022;34(12):2018–2035e8.
- 19. Urra H, Dufey E, Avril T, Chevet E, Hetz C. Endoplasmic Reticulum Stress and the Hallmarks of Cancer. Trends Cancer. 2016;2(5):252–62.
- 20. Hetz C. The unfolded protein response: controlling cell fate decisions under ER stress and beyond. Nat Rev Mol Cell Biol. 2012;13(2):89–102.
- 21. Malhi H, Kaufman RJ. Endoplasmic reticulum stress in liver disease. J Hepatol. 2011;54(4):795–809.
- 22. Kondratyev M, Avezov E, Shenkman M, Groisman B, Lederkremer GZ. PERK-dependent compartmentalization of ERAD and unfolded protein response machineries during ER stress. Exp Cell Res. 2007;313(16):3395–407.
- 23. Rzymski T, Milani M, Singleton DC, Harris AL. Role of ATF4 in regulation of autophagy and resistance to drugs and hypoxia. Cell Cycle. 2009;8(23):3838–47.
- 24. Wu J, Kaufman RJ. From acute ER stress to physiological roles of the Unfolded Protein Response. Cell Death Differ. 2006;13(3):374–84.
- 25. Hetz C, Chevet E, Harding HP. Targeting the unfolded protein response in disease. Nat Rev Drug Discov. 2013;12:703–19.
- 26. Wang H, Zhang G. Endoplasmic reticulum stress-mediated autophagy protects against β,β-dimethylacrylshikonin-induced apoptosis in lung adenocarcinoma cells. Cancer Sci. 2018;109(6):1889–901.
- 27. Brem GJ, Mylonas I, Brüning A. Eeyarestatin causes cervical cancer cell sensitization to bortezomib treatment by augmenting ER stress and CHOP expression. Gynecol Oncol. 2013;128(2):383–90.

- 28. Cheng WC, Wen Y, Chiu YS, Chou CH, Lim CJ, Lin SH, Chang JM, Lin CC. Pendulone induces apoptosis via the ROS-mediated ER-stress pathway in human non-small cell lung cancer cells. Toxicol In Vitro. 2022;81:105346.
- 29. Wang S, Fu JL, Hao HF, Jiao YN, Li PP, Han SY. Metabolic reprogramming by traditional Chinese medicine and its role in effective cancer therapy. Pharmacol Res. 2021;170:105728.
- 30. Li Z, Feiyue Z, Gaofeng L. Traditional Chinese medicine and lung cancer–From theory to practice. Biomed Pharmacother. 2021;137:111381.

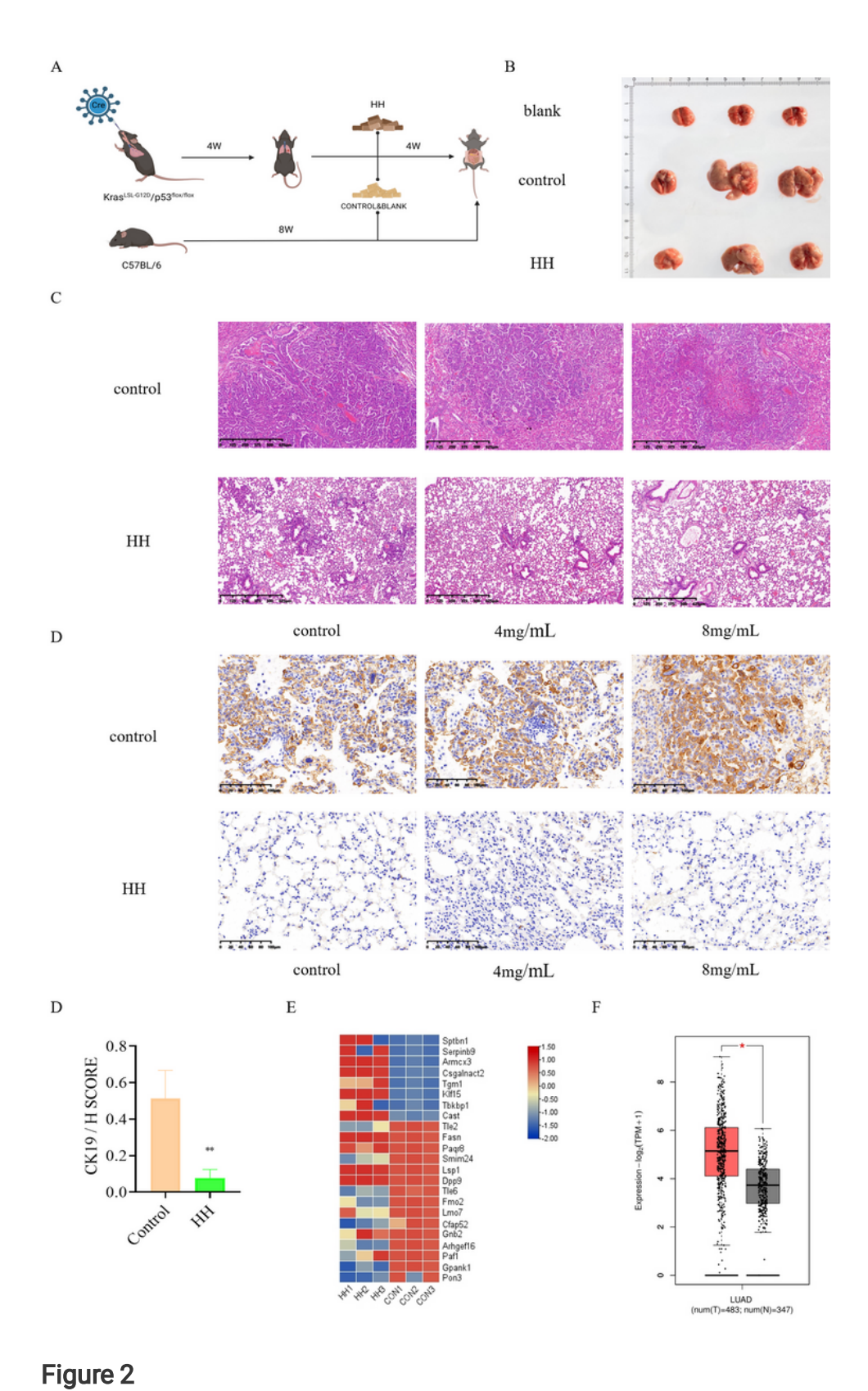
Figures



Pharmacological Analysis Network of HH and HH inhibits lung cancer cell proliferation

- (A) Sample of Scutellaria baicalensis and Polygonatum
- (B) Assessment of the correlation between HH and lung cancer in the symmap database

- (C) Network pharmacological research of the anti-cancer target of HH. Blue—the active ingredients of Polygonatum; Green—the active ingredients of SB; Pink—Common targets for HH interactions.
- (D) Venn diagram of HH and lung cancer based on TCMSP, drugbank, OMIM and GeenCards databases.
- (E) Inhibition rate of cell viability after HH treatment at a concentration of 0, 2, 4, 8, 16 mg/mL in A549 cells.
- (F) Measurement of IC $_{50}$ values by CCK8 test after 24h of intervention A549 for SB and Polygonatum respectively (**P < 0.01 and ****P 0.001). The data represent similar results from three parallel experiments.
- (G) Morphological changes in lung cancer cells after HH treatment 20× and Determination of the number of A549 cells interfered with by different concentrations of HH by cell counter (****P 0.001). The data represent similar results from three parallel experiments.



HH suppresses tumor growth in vivo

- (A) Experimental design of the study in Kras $^{LSL\text{-}G12D}$ /p53 $^{flox/flox}\,$ and C57BL/6 mice.
- (B) Images of lung tissues after 4 weeks HH treatment

- (S1) Body weight after treatment with HH at different days
- (C) HE-stained lung tissue section under a 4× phase contrast microscope
- (D) Lung tissue after CK19 IHC staining by under a 20× phase contrast microscope and the Histochemistry score (H-Score) was used to convert the number of positive lung tumours and their staining intensity within each section into a corresponding value for the purpose of semi-quantification of tissue staining. the higher the H-score value the stronger the combined positive intensity. the H-Score in the HH group was significantly lower than that in the control group (p < 0.01)
- (S2) Volcano mapping of differential genes by proteomic analysis of lung tissue between HH and control group.
- (E) Heatmap of more differentially expressed proteins in HH and control groups. Red: Up-regulated proteins in HH; Blue: Down-regulated proteins in HH.
- (F) Expression in normal people and lung adenocarcinoma patients from TCGA database. Red: PON_3 expression in lung adenocarcinoma patients; Black: PON_3 expression in normal people. PON_3 expression in lung adenocarcinoma patients was significantly increased compared with that in normal people.
- (S3) Analysis of PON3 expression in different cancer populationsz based on the GEPIA database.

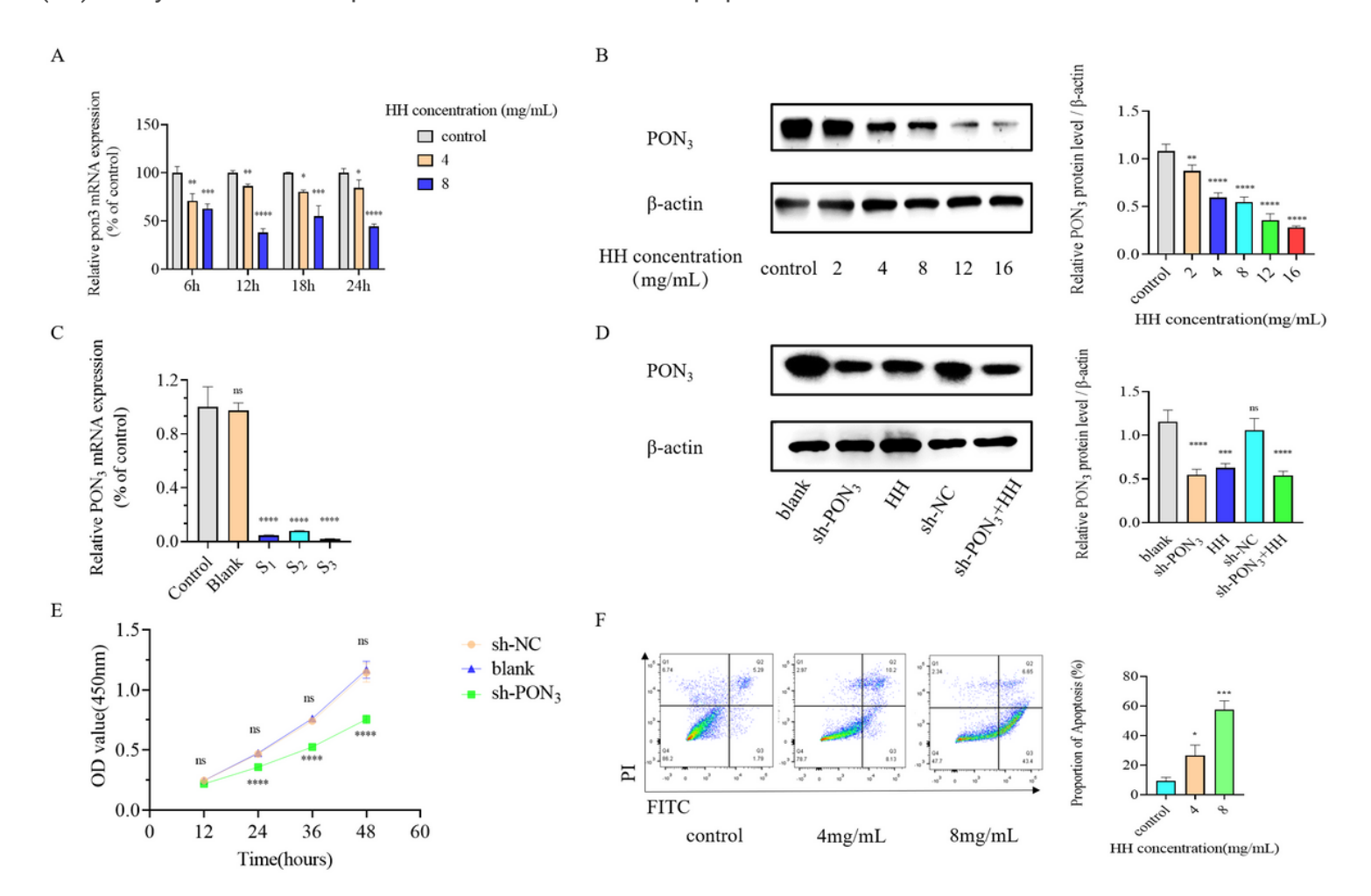


Figure 3

HH inhibits the expression of PON₃ and induces apoptosis

- (A) PON_3 expression detected by qPCR assay after different time periods HH treatment at a concentration of 4mg/mL or 8mg/mL (***P < 0.001 and ****P < 0.0001).
- (B) Western blot analysis of PON_3 after 24 h HH treatment at different concentrations and the PON_3 protein levels were quantified (**P < 0.01 and ****P < 0.0001).
- (C) The mRNA levels of PON_3 were significantly reduced after 24h of the three types of siRNA-mediated knockdown. (****P < 0.0001)
- (D) Analysis of PON_3 's protein expression levels in the HH, sh- PON_3 and HH+sh- PON_3 groups by western blot and data are representative of at least three separate experiments and presented as the means±SD. ***P < 0.001 and ****P < 0.0001 versus blank.
- (E) Proliferation was detected using CCK-8 after incubation with sh-PON $_3$ ((****P 0.001 vs sh-PON $_3$) or blank)).
- (F) After various concentrations of HH treatment, A549 cells were double-labeled with Annexin V/PI and analyzed by flow cytometry. Quantitative analysis of the total apoptotic cells is shown in histograms (*P < 0.05 and ****P 0.001). The data represent similar results from three parallel experiments.

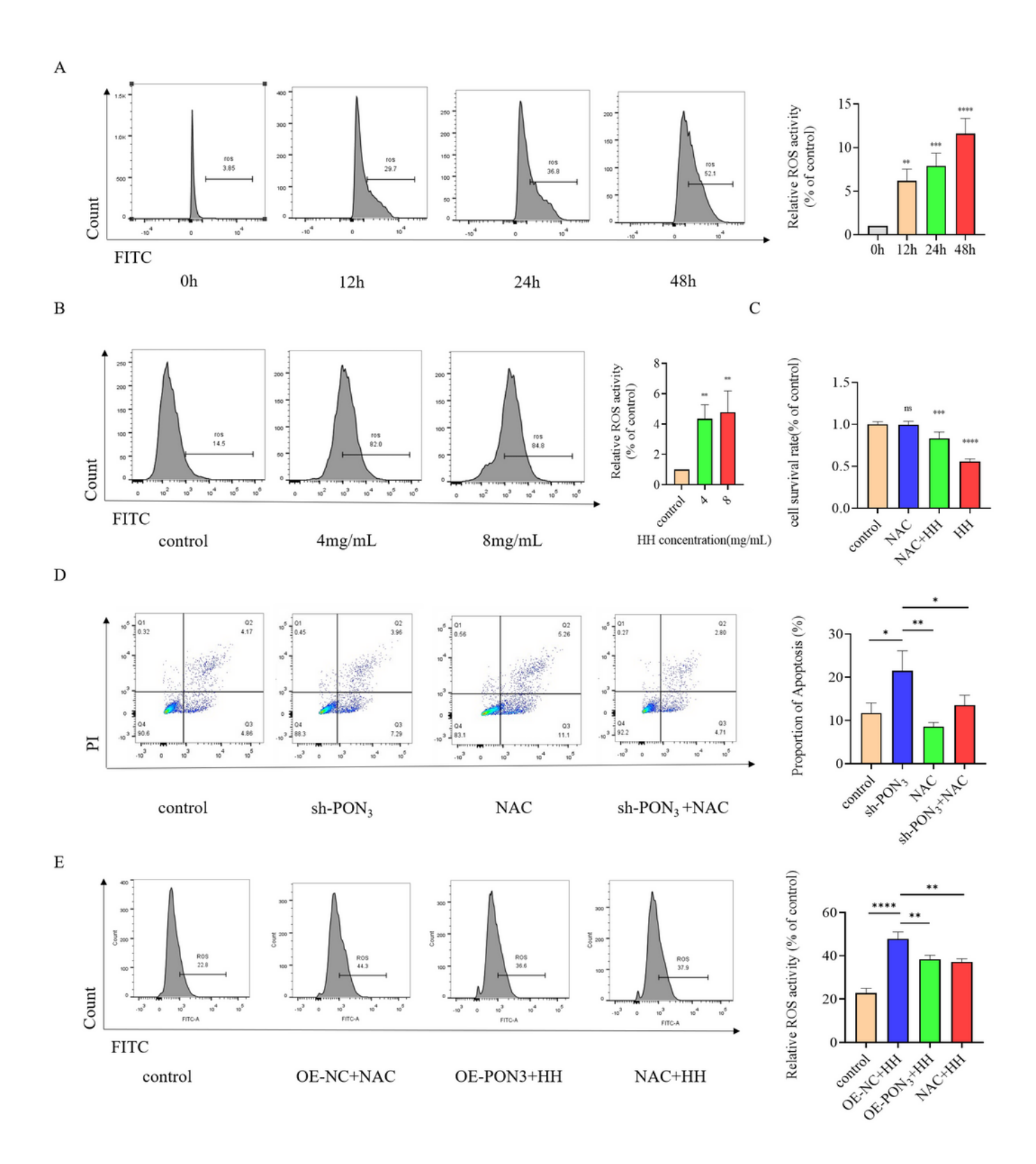


Figure 4

HH induces apoptosis via ROS in A549 cells

(A) A549 cells were treated with 4mg/mL HH for various times (0, 12, 24, 48h), stained with DCFH-DA and measured by flow cytometry. Each bar represents the means \pm SD from three experiments. **P < 0.01, ***P < 0.001 and ***P < 0.0001 versus 0h HH treatment.

- (B) A549 cells were treated with various concentrations of HH for 24 h, stained with DCFH-DA and measured using flow cytometry. Data are representative of at least three separate experiments and presented as the means \pm SD. **P < 0.01 versus control.
- (C) A549 cells were pretreated 4mg/mL HH with or without $200\mu M$ NAC for 24 h. Cell viability was measured using CCK8 analysis. The data represent similar results from three independent experiments. (***P < 0.001 and ****P 0.0001)
- (D) Apoptosis rates of A549 cells induced by siRNA (PON_3) and NAC. The NAC concentration is $200\mu M$. Intervention with NAC and siRNA (PON_3) separately and in combination for 24 h was stained with membrane linked protein FITC / PI and analysed by flow cytometry. Data are presented as the means±SD of three separate experiments (*P< 0.05 and **P< 0.01 vs. blank).
- (E) Plasmids overexpressing PON_3 were transfected into A549 cells after co-incubation at 4 mg/mL of HH intervention for 24 h and compared to the added NAC group, stained with DCFH-DA and measured by flow cytometry. Data are representative of at least three independent experiments and are expressed as mean \pm SD. (**P<0.01 and ****P<0.0001)

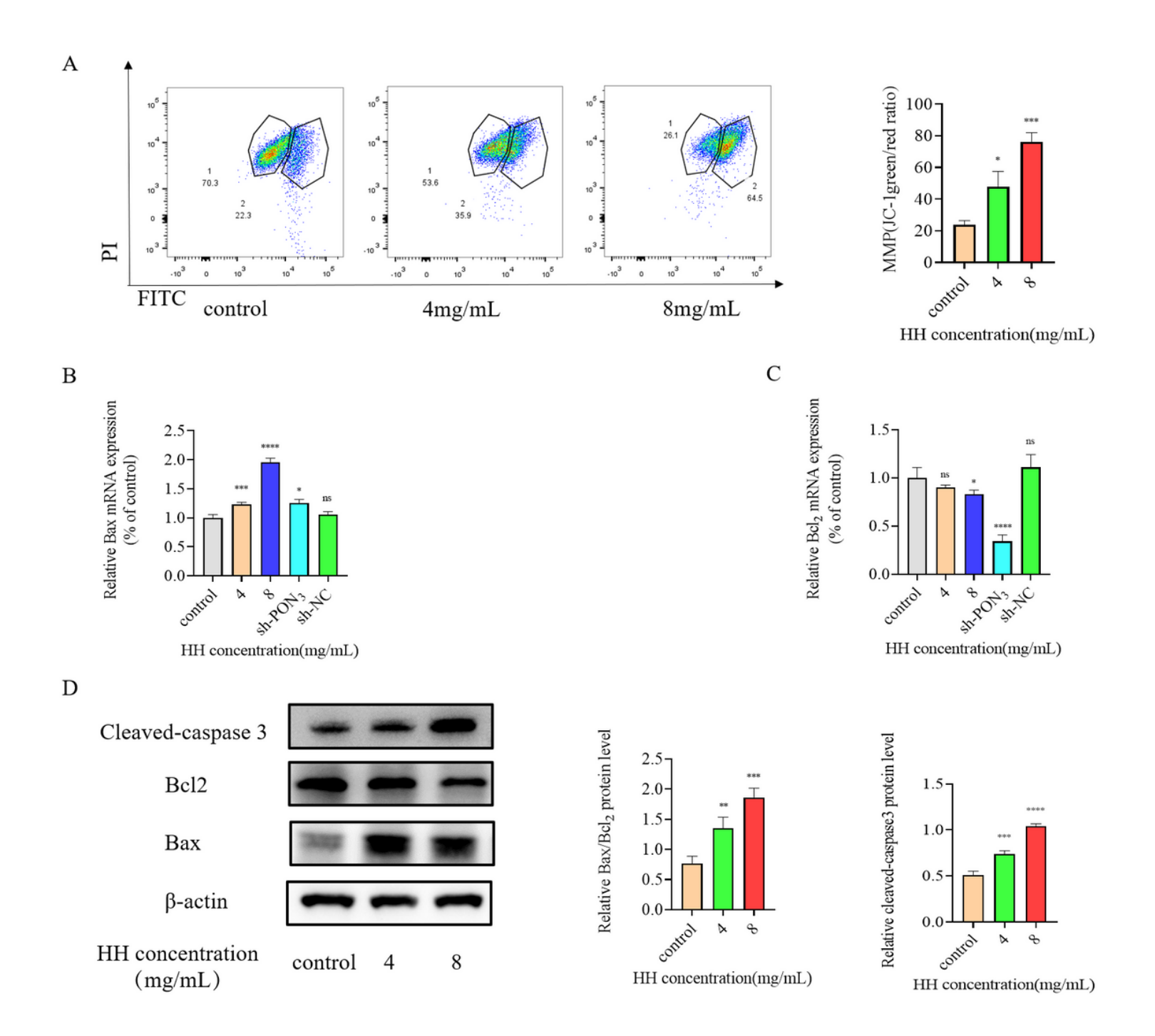


Figure 5 HH apoptosis by the mitochondrial pathway via PON_3

- (A) Measurement of the $\Delta\Psi m$ in cells after 24h HH treatment. The mitochondrial membrane potential (MMP) was analyzed by flow cytometry using JC-1 fluorescent dye staining. The bar graphs of the percentage of JC-1 aggregates show the mean \pm SD of 3 wells from a representative experiment. *P < 0.05 and ***p < 0.001, significantly different compared with the control group (one-way ANOVA).
- (B-C) Expression of Bax and Bcl₂ expression and their expression after knockdown of PON₃ detected by qPCR assay after 24h HH treatment at a concentration of 4mg/mL.

(D) Western blot analysis of Bcl2, Bax, cleaved-caspase 3 after 24h HH treatment at different concentrations. The protein levels were quantified (**P < 0.01, ***p < 0.001 and ***p < 0.001).

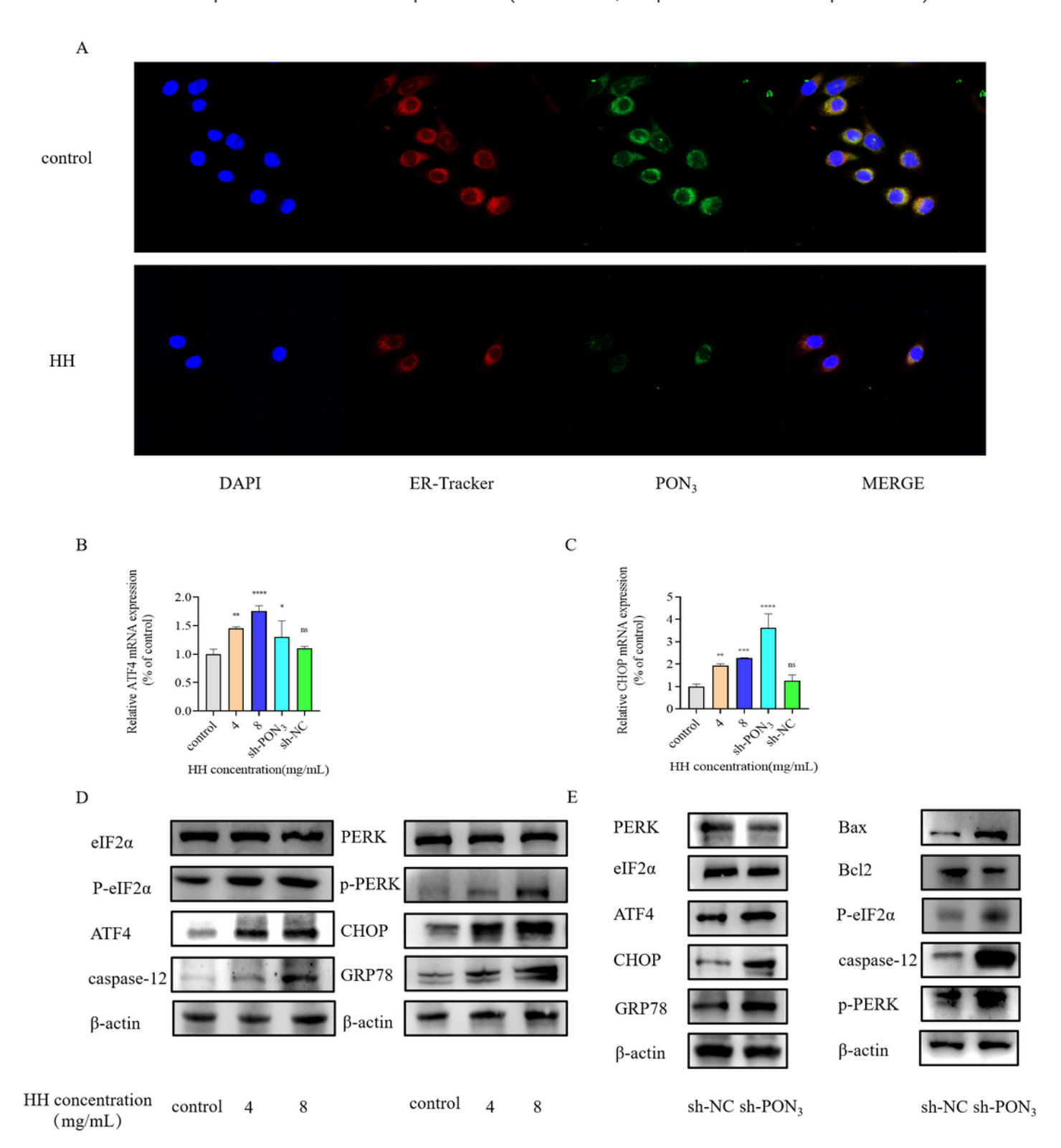
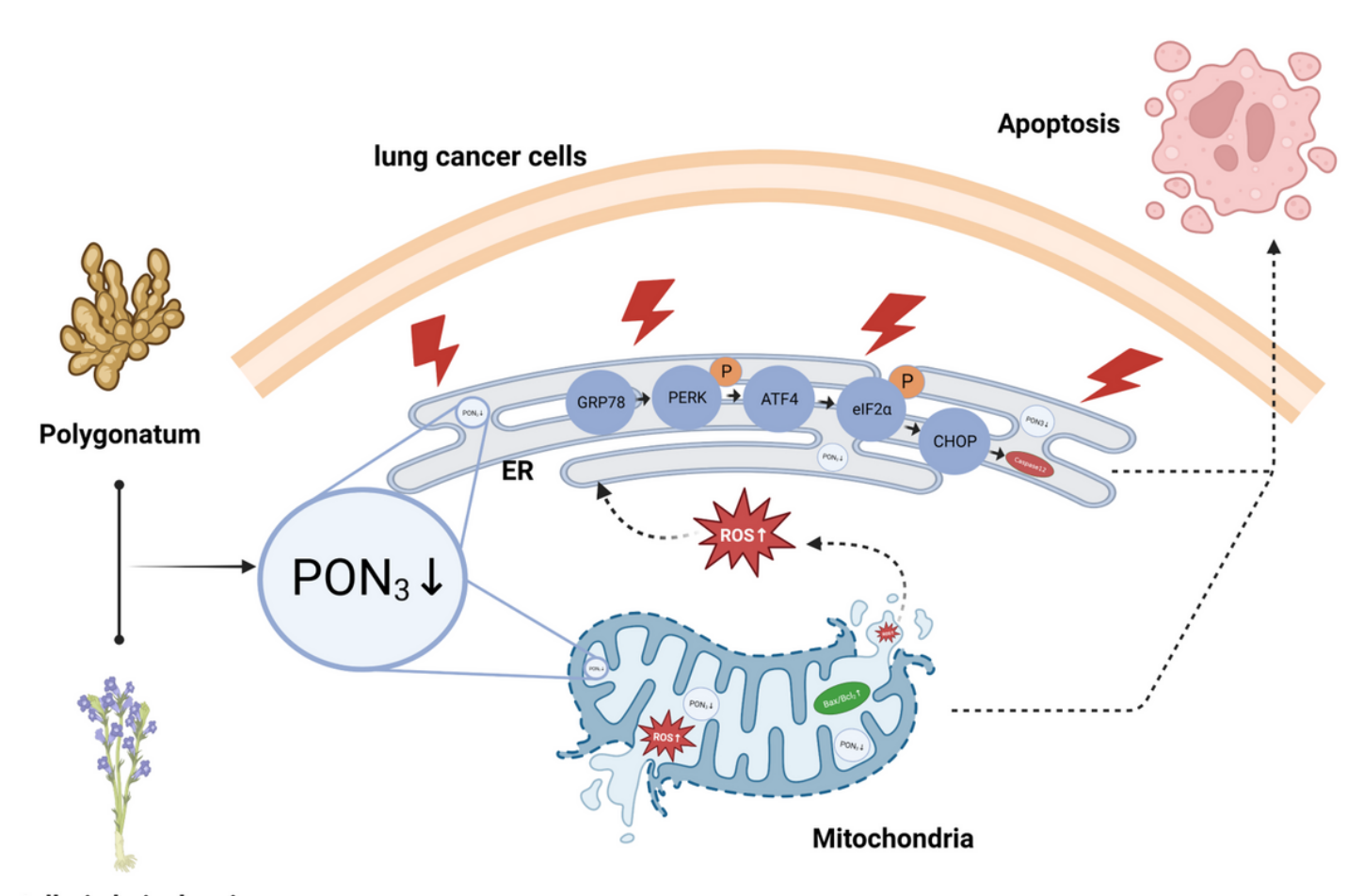


Figure 6

HH induces apoptosis by triggering endoplasmic reticulum stress via PON₃

- (A) Representative images obtained by confocal fluorescence microscopy stained with PON_3 antibody in ER. The data shown are representative of three independent experiments with similar results. Scale bars: 10 μm
- (B-C) Expression of ATF4 and CHOP expression and their expression after knockdown of PON_3 detected by qPCR assay after 24h HH treatment at a concentration of 4mg/mL.
- (D) Western blot analysis of ER stress-related protein after 24h HH treatment.
- (E) The effects of PON₃ knockdown on the expression of different protein were ascertained by western blot.



Scutellaria baicalensis

Figure 7

Schematic representation of the role of HH in inducing apoptosis in lung cancer cells via ER stress and the mitochondrial pathway

Supplementary Files

This is a list of supplementary files associated with this preprint. Click to download.

- S1.png
- S2.png
- S3.png